

Quantum Monte Carlo and exact diagonalization study of a dynamic Hubbard model

J. E. Hirsch

Department of Physics, University of California, San Diego, La Jolla, California 92093-0319

(Received 31 December 2001; revised manuscript received 3 April 2002; published 22 May 2002)

A one-dimensional model of electrons locally coupled to spin-1/2 degrees of freedom is studied by numerical techniques. The model is one in the class of *dynamic Hubbard models* that describe the relaxation of an atomic orbital upon double-electron occupancy due to electron-electron interactions. We study the parameter regime where pairing occurs in this model by exact diagonalization of small clusters. World-line quantum Monte Carlo simulations support the results of exact diagonalization for larger systems and show that the kinetic energy is lowered when pairing occurs. The qualitative physics of this model and others in its class, obtained through approximate analytic calculations, is that superconductivity occurs through hole undressing even in parameter regimes where the effective on-site interaction is strongly repulsive. Our numerical results confirm the expected qualitative behavior and show that pairing will occur in a substantially larger parameter regime than predicted by the approximate low-energy effective Hamiltonian.

DOI: 10.1103/PhysRevB.65.214510

PACS number(s): 74.20.Mn, 71.10.Fd

I. INTRODUCTION

Dynamic Hubbard models have been recently introduced as a new class of model Hamiltonians to describe the relaxation of atomic orbitals when electrons are added to orbitals already occupied by other electrons.¹⁻³ This process, originating in the strong on-site repulsion between electrons in the same atomic orbital, is not described by the conventional Hubbard model.⁴ In dynamic Hubbard models this physics is represented either by introducing auxiliary spin⁵ or oscillator⁶ degrees of freedom, or by adding a second electronic orbital to the site Hilbert space,⁷ with suitable interaction parameters. As a consequence, the on-site Hubbard repulsion becomes a dynamical variable and can take a range of values rather than a single fixed value as in the static (conventional) Hubbard model. It has been proposed that this physics is ubiquitous to electrons in atoms, molecules, and solids^{1-3,8} and that it is relevant to the understanding of superconductivity in nature.⁹

While a vast amount of work has been performed over the years on the conventional Hubbard model,^{10,11} very little work has been done so far on dynamic Hubbard models. It is known^{12,6,7} that in the strong-coupling antiadiabatic limit these models map onto the Hubbard model with correlated hopping, i.e., a Hubbard model where the electronic hopping amplitude depends on the occupation of the two sites involved in the hopping process. This model is known to exhibit superconductivity when the Fermi level is close to the top of the band, both from mean-field calculations,¹³⁻¹⁵ exact diagonalization,¹⁶⁻¹⁸ and other exact techniques.^{19,20} Furthermore, a variety of observable properties have been calculated in this limit such as thermodynamics,^{13,21} tunneling,²² optical properties,²³ pressure dependence,²¹ etc. Because superconductivity occurs in the dilute carrier concentration regime, it is believed that these BCS mean-field calculations are reliable.²⁴

The antiadiabatic limit of these models occurs when the frequency of the associated boson degree of freedom, ω_0 , is much larger than the effective hopping amplitude for the electrons (small-polaron regime²⁵), where the boson follows

the electronic motion. In that limit the parameter regime where pairing occurs can be calculated exactly for a dilute concentration of hole carriers.²⁴ Furthermore, numerical calculations on finite clusters show that the doping regime where pairing occurs is accurately estimated by BCS theory.¹⁸ For finite frequency ω_0 , some numerical results have been reported.^{5,12} However, it is generally not known whether finite ω_0 enhances or reduces the tendency to pairing.

Furthermore, in the antiadiabatic limit the single carriers have large effective mass, and the effective mass is lowered when carriers pair.^{26,27} The resulting gain in kinetic energy drives superconductivity.²⁸ It is not known whether this physics exists beyond the antiadiabatic limit.

In this paper we study a particular realization of a dynamic Hubbard model, with an auxiliary spin degree of freedom, by exact diagonalization of small clusters and a quantum Monte Carlo method, to shed light on the properties of the model away from the antiadiabatic limit. We believe that similar qualitative behavior may be found in the entire class of dynamic Hubbard models. Briefly, our results show that the qualitative physics of the antiadiabatic limit persists for finite ω_0 and that the parameter regime where pairing occurs can be substantially larger. Even though our results are for a one-dimensional system, we believe it is likely that the same occurs in higher dimensions.

The model studied here bears some superficial resemblance to electron-boson models that have been extensively studied in the past such as the Holstein model.²⁵ However, its physics is qualitatively different. To illustrate this point we present some numerical results for an electron-hole symmetric model with an auxiliary spin degree of freedom coupled to the electronic site density. This model is expected to be similar to the Holstein model and exhibits qualitatively different physics to the dynamic Hubbard model.

The paper is organized as follows. Section II defines the model and discusses its properties in the antiadiabatic limit. In Sec. III we present results for the effective interaction and kinetic energy from diagonalization of small clusters, and Sec. IV discusses results of world-line quantum Monte Carlo

simulations. In Sec. V we present and discuss results for the electron-hole symmetric Holstein-like model. Section VI discusses the relation between the dynamic Hubbard model studied here for a site and a real atom. We conclude in Sec. VII with a summary of our results and a discussion of the many open questions in this area.

II. DYNAMIC HUBBARD MODEL WITH SPIN-1/2 DEGREE OF FREEDOM

The essence of dynamic Hubbard models is electron-hole symmetry breaking at the local (one-site) level, so that the dressing of a hole is larger than the dressing of an electron.³ This physics originates in the dynamic lowering of the on-site repulsion U when a second electron is added to an atomic orbital, due to rearrangement of the first electron, and is a ubiquitous phenomenon in atoms.² There are a variety of dynamic Hubbard models that can be constructed with an auxiliary spin-1/2 degree of freedom.^{1,3} Here we consider the site Hamiltonian for *electrons*

$$H_i = \omega_0 \sigma_x^i + g \omega_0 \sigma_z^i + [U - 2g \omega_0 \sigma_z^i] n_{i\uparrow} n_{i\downarrow}. \quad (1a)$$

Hence, for zero and one electrons (one and two holes) at the site, the site Hamiltonian is

$$H_i(n_i < 2) = \omega_0 \sigma_x^i + g \omega_0 \sigma_z^i \quad (1b)$$

and for two electrons (zero holes) at the site it is (spin part only)

$$H_i(n_i = 2) = \omega_0 \sigma_x^i - g \omega_0 \sigma_z^i. \quad (1c)$$

Equation (1a) can be written in hole representation as

$$H_i = \omega_0 \sigma_x^i + g \omega_0 [2(n_{i\uparrow} + n_{i\downarrow}) - 1] \sigma_z^i + [U - 2g \omega_0 \sigma_z^i] n_{i\uparrow} n_{i\downarrow} \quad (2)$$

(omitting a chemical potential term), and the lattice Hamiltonian is

$$H = \sum_i H_i - t \sum_{i,\sigma} [c_{i\sigma}^\dagger c_{i+1,\sigma} + \text{H.c.}] \quad (3)$$

in either electron or hole representation. The electron-hole transformation is $c_{i\sigma}^\dagger \rightarrow (-1)^i c_{i\sigma}$.

A. Site Hamiltonian

We will use the Hamiltonian in the hole representation, Eq. (2). The site eigenstates when there are n holes at the site are, in terms of the spin-1/2 σ_z eigenstates $|+\rangle$, $|-\rangle$,

$$|n\rangle = u(n)|+\rangle + v(n)|-\rangle, \quad (4a)$$

$$|\bar{n}\rangle = v(n)|+\rangle - u(n)|-\rangle, \quad (4b)$$

with eigenvalues (excluding the σ -independent term in H_i)

$$\epsilon(n) = -\epsilon(\bar{n}) = -\omega_0 \sqrt{1+g^2} \quad (5)$$

and

$$u^2(0) = \frac{1}{2} \left(1 + \frac{g}{\sqrt{1+g^2}} \right), \quad (6a)$$

$$v^2(0) = \frac{1}{2} \left(1 - \frac{g}{\sqrt{1+g^2}} \right), \quad (6b)$$

$$u(0)v(0) = -\frac{1}{2\sqrt{1+g^2}}, \quad (6c)$$

$$\frac{u(0)}{v(0)} = g - \sqrt{1+g^2} \quad (6d)$$

and

$$u(1) = u(2) = v(0), \quad (7a)$$

$$v(1) = v(2) = u(0). \quad (7b)$$

Hence the ground-state energy is independent of the electronic site occupation in this model. The site eigenfunctions depend on g , but not on ω_0 , and are the same for site occupation $n=1$ and $n=2$, and different for $n=0$. For large g the ground-state wave functions are almost eigenstates of σ_z , with $\sigma_z \sim -1$ for one-hole and two-hole occupation, very different from the one for zero hole occupation for which $\sigma_z \sim +1$, while for small g the ground-state wave function is almost an eigenstate of σ_x ($\sigma_x \sim -1$) and similar for the different hole occupations. The site eigenvalues depend on both g and ω_0 .

The on-site repulsion between two holes (or two electrons) at the same site depends on the state of the spin degree of freedom and can range between $U + 2g\omega_0$ and $U - 2g\omega_0$. The effective on-site repulsion, however, since the ground-state energy, Eq. (5), is independent of occupation, is simply U . Note that our notation here is different from that of Ref. 2, where U denoted the *bare* on-site repulsion; here, the bare on-site repulsion, which is the on-site repulsion if the background degree of freedom is not allowed to relax upon double occupancy, is

$$U_{bare} = U + \frac{2g^2\omega_0}{\sqrt{1+g^2}} \quad (8)$$

or $U_{bare} \sim U + 2g\omega_0$ for large g . Finally, the overlap matrix elements between the ground-state wave functions for the various hole occupations are

$$\langle 0|1\rangle = 2u(0)v(0) = \frac{1}{\sqrt{1+g^2}} \equiv S, \quad (9a)$$

$$\langle 1|2\rangle = 1. \quad (9b)$$

B. Effective low-energy Hamiltonian

The effective hopping amplitude for a hole between neighboring sites if the spin degree of freedom makes a ground-state to ground-state (diagonal) transition is

$$t_2 = |\langle 0|1\rangle|^2 t = S^2 t = \frac{t}{1+g^2} \quad (10a)$$

if there are no other holes in the two sites involved in the hopping process. Instead, if there are either one or two other holes of opposite spins, the hopping amplitudes are

$$t_1 = |\langle 0|1\rangle\langle 1|2\rangle| = St, \quad (10b)$$

$$t_0 = |\langle 1|2\rangle|^2 t = t, \quad (10c)$$

respectively. The low-energy effective Hamiltonian for holes in the small-polaron regime is then

$$H_{eff} = - \sum_{i,\sigma} t_{i,i+1}^\sigma (c_{i\sigma}^\dagger c_{i+1,\sigma} + \text{H.c.}) + U \sum_i n_{i\uparrow} n_{i\downarrow}, \quad (11a)$$

$$t_{ij}^\sigma = t [S^2 + S(1-S)(n_{i,-\sigma} + n_{j,-\sigma}) + (1-S)^2 n_{i,-\sigma} n_{j,-\sigma}]. \quad (11b)$$

In the regime of low hole concentration the hopping processes where more than two holes are in the sites involved can be neglected, and the effective Hamiltonian is the Hubbard model with correlated hopping.¹³

$$H_{eff} = - \sum_{i,\sigma} [t_2 + \Delta t (n_{i,-\sigma} + n_{i+1,-\sigma})] \times (c_{i\sigma}^\dagger c_{i+1\sigma} + \text{H.c.}) + U \sum_i n_{i\uparrow} n_{i\downarrow}, \quad (12a)$$

$$\Delta t = t_1 - t_2 = tS(1-S). \quad (12b)$$

The binding energy of the polaron is obtained from the difference of $\epsilon(0)$ and the expectation value of H_i if the spin does not adjust to the presence of a carrier and yields

$$\epsilon_p = \frac{2\omega_0 g^2}{\sqrt{1+g^2}}. \quad (13)$$

The criterion for small-polaron formation is that the energy of the polaron be smaller than that of a carrier that moves without changing the spin background:

$$z(t - t_2) < \epsilon_p, \quad (14)$$

with z the number of nearest neighbors to a site ($z=2$ in one dimension). Equation (14) yields

$$t < \frac{2\omega_0}{z} \sqrt{1+g^2} \quad (15)$$

as the condition for polaron formation. For the hopping of a single polaron, the antiadiabatic limit is valid if the polaron hopping amplitude t_2 is smaller than the spacing between site energy levels; hence,

$$t < \omega_0 (1+g^2)^{3/2}, \quad (16)$$

which is always satisfied if the condition, Eq. (15), is satisfied.

The condition, Eq. (15), indicates that the small-polaron regime will occur when *either* ω_0 is large *or* the coupling g is large. However, the condition, Eq. (15), is *not* sufficient for the effective Hamiltonian, Eq. (11) or (12), to be accurate in the presence of more than one carrier. Virtual transitions of a hole to a nearest-neighbor site occupied by another hole yield a contribution to the effective interaction between holes with an amplitude of the form

$$\frac{|\langle 1|\bar{0}\rangle|^2}{\epsilon(\bar{0}) + \epsilon(2) - 2\epsilon(1) + U} = \frac{g^2}{1+g^2} \frac{1}{U + 2\omega_0 \sqrt{1+g^2}} \quad (17)$$

from ‘‘vertical’’ transitions, which can be much larger than the second-order contribution from the effective Hamiltonian, Eq. (11), that describes only diagonal transitions:

$$\frac{|\langle 1|0\rangle|^2}{\epsilon(0) + \epsilon(2) - 2\epsilon(1) + U} = \frac{1}{(1+g^2)U}. \quad (18)$$

These contributions from vertical transitions can be neglected if Eq. (17) is smaller than Eq. (18), which yields the condition

$$\omega_0 \sqrt{1+g^2} > U \frac{(g^2-1)}{2} \quad (19a)$$

or, for large g ,

$$\omega_0 > \frac{Ug}{2}. \quad (19b)$$

Only when *both* conditions, Eqs. (15) and (19), hold can the effective low-energy Hamiltonian, Eq. (11) or (12), be expected to be accurate. In particular, for large g and small ω_0 Eq. (15) may hold and Eq. (19) may not. In that case, the effective Hamiltonian, Eq. (11), can be expected to *underestimate* the tendency to pairing due to its complete neglect of the site excited states. The antiadiabatic limit where the effective Hamiltonian, Eq. (11), is valid hence occurs for $\omega_0 \rightarrow \infty$ for fixed g but not for $g \rightarrow \infty$ for fixed ω_0 . As g increases it is seen from the condition, Eq. (19), that the antiadiabatic limit will be attained for larger ω_0 .

C. Pairing condition and effective mass in antiadiabatic limit

The condition on the parameters of the Hamiltonian, Eq. (12), to yield pairing of two holes in a full band is (in one and two dimensions) (Ref. 24)

$$\frac{\Delta t}{t_2} > \sqrt{1 + \frac{U}{D_h}} - 1, \quad (20)$$

with $D_h = 2zt_2$ the single-carrier renormalized bandwidth. This is also the condition for superconductivity within BCS theory in the dilute limit in any dimension.¹³ Using Eqs. (12b) and (10a) it translates into

$$\frac{U}{D_h} \leq g^2, \quad (21)$$

which shows that for $g > 1$ pairing will occur even if the on-site repulsion is larger than the effective bandwidth. Equation (21) can also be written as

$$\frac{U}{D} \leq \frac{g^2}{1+g^2}, \quad (22)$$

with $D = 2zt$ the unrenormalized bandwidth.

The polaron hopping amplitude increases as the hole filling of the band increases, according to

$$t(n_h) = t_2 + n_h \Delta t, \quad (23)$$

with n_h the average number of holes per site ($0 \leq n_h \leq 2$), and correspondingly the bandwidth increases,

$$D(n_h) = D_h \left(1 + n_h \frac{\Delta t}{t_2} \right), \quad (24)$$

from $D(n_h=0) = D_h$ to $D(n_h=2) = D$. The polaron effective mass correspondingly decreases as the number of holes increases,

$$m^*(n_h) = \frac{\hbar^2}{2t(n_h)a^2}, \quad (25)$$

with a the lattice spacing.

When two holes bind in a pair, the pair hopping amplitude t_p in the dilute hole concentration regime is found to be always larger than 1/2 the single-particle hopping amplitude,

$$t_p > t_2/2; \quad (26)$$

i.e., the pair effective mass is smaller than the sum of the effective masses of its constituents.²⁷ This is opposite to what happens in other models such as the attractive Hubbard model. Expressions for the pair mobility t_p are given in Refs. 26 and 27. The pair mobility is defined in terms of the energy dispersion relation for a pair of center-of-mass momentum q ,

$$E(q) = E_0 + t_p q^2, \quad (27)$$

and can be obtained by calculating the London penetration depth in the dilute limit. The kinetic energy per two holes in the dilute limit when there is no pairing is

$$\langle T_s \rangle = -4t_2, \quad (28a)$$

and when there is pairing the kinetic energy per pair is

$$\langle T_p \rangle = -8t_p \quad (28b)$$

for a one-dimensional chain.

III. EXACT DIAGONALIZATION RESULTS

The Hamiltonian of interest has eight states per site, so that clusters of up to eight sites could be studied with current computer capabilities. In this initial study we restrict ourselves to two and four sites only. The results are qualitatively similar and we expect similar qualitative results for larger clusters, although quantitative differences may be expected for weak coupling. We compute the effective interaction for

two holes in a cluster from the usual formula

$$U_{eff} = 2E_0(1) - E_0(0) - E_0(2), \quad (29)$$

with $E_0(n_h)$ the ground-state energy for n_h holes; $U_{eff} < 0$ signals a tendency to pairing and superconductivity. For the $N=2$ cluster the effective interaction in the antiadiabatic limit is

$$U_{eff} = \frac{U}{2} - \sqrt{\left(\frac{U}{2}\right)^2 + 4t_1^2 - 2t_2}, \quad (30a)$$

$$t_1 = t_2 + \Delta t = tS, \quad (30b)$$

and the condition for pairing ($U_{eff} < 0$) is

$$\frac{U}{2t} \leq \frac{g^2}{1+g^2}, \quad (31)$$

so that in the antiadiabatic limit pairing cannot occur for $U > 2t$ for any value of the coupling parameter g . Throughout this and the following section we will use units so that $t = 1$. For the $N=4$ system and in fact for any $N \geq 4$, the condition for pairing in the antiadiabatic limit is

$$\frac{U}{4t} \leq \frac{g^2}{1+g^2}, \quad (32)$$

so that pairing will not occur for $U > 4$ for any g in the limit $\omega_0 \rightarrow \infty$.

A. Results for effective interaction

Figure 1 shows the effective interaction for the $N=4$ cluster as function of coupling constant g , for various values of the on-site repulsion U and two values of the frequency ω_0 , together with the results in the antiadiabatic limit. Note that for small ω_0 [Fig. 1(a)] the effective interaction is substantially more attractive than in the antiadiabatic limit. As ω_0 increases [Fig. 1(b)] the results approach those of the antiadiabatic limit, as expected. The behavior of U_{eff} versus g is nonmonotonic particularly for small values of U .

In Fig. 2 we show the dependence of the effective interaction on ω_0 for the $N=4$ cluster for fixed $U=4$ and various values of g (a) and for fixed g for various values of U (b). The limiting values for $\omega_0 \rightarrow \infty$ are also shown (dashed lines). For $U=4$ there is no pairing in the antiadiabatic limit, while Fig. 2(a) shows that for finite frequency pairing will occur for $g \geq 2$. Similarly, Fig. 2(b) shows that for $g=3$ (corresponding to an effective mass enhancement $m^*/m = 1 + g^2 = 10$) pairing will occur up to at least $U=6$ at finite ω_0 , while in the antiadiabatic limit $U=3.6$ is the maximum on-site repulsion that allows pairing for $g=3$ according to Eq. (32). Note that for larger g the antiadiabatic limit is approached for larger ω_0 , in accordance with the discussion following Eq. (19).

Even a cluster as small as $N=2$ shows behavior representative of larger clusters and of (we believe) the thermodynamic limit. The reader can easily verify that the effective interaction for the $N=2$ cluster obtained by exact diagonalization closely resembles the behavior of the four-site cluster

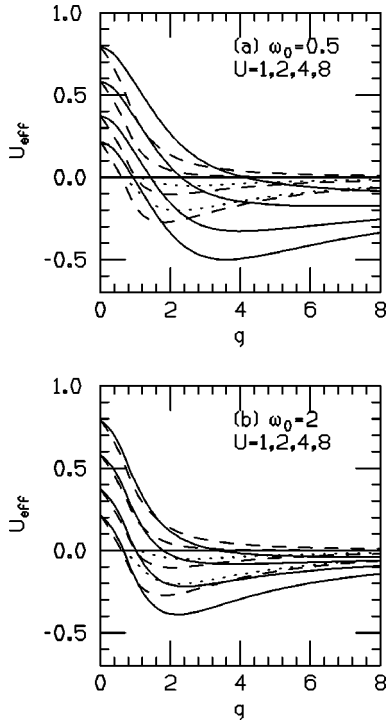


FIG. 1. Effective interaction U_{eff} for $N=4$ cluster vs coupling constant g and various values of the on-site repulsion U for (a) $\omega_0=0.5$ and (b) $\omega_0=2$ (solid lines). The dashed lines and dotted lines give the results in the $\omega_0 \rightarrow \infty$ limit for the $N=4$ cluster and for the infinite chain, respectively. For fixed g , increasing U corresponds to increasing value of U_{eff} .

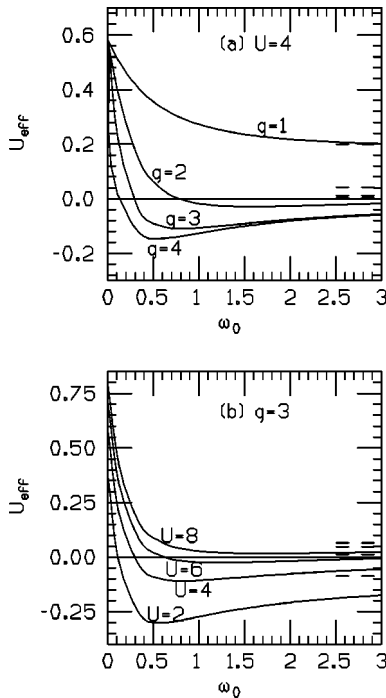


FIG. 2. Dependence of U_{eff} on ω_0 for $N=4$ cluster. The dashed lines give the limiting values $\omega_0 \rightarrow \infty$.

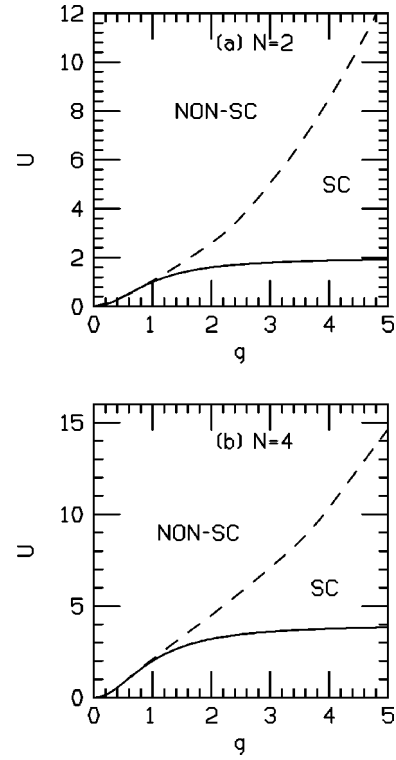


FIG. 3. Phase diagram for (a) $N=2$ and (b) $N=4$ clusters. In the region labeled NON-SC, $U_{eff} > 0$ for all values of ω_0 ; in the region labeled SC, a range of ω_0 exists where $U_{eff} < 0$. Below the solid line, $U_{eff} < 0$ in the antiadiabatic limit $\omega_0 \rightarrow \infty$.

shown in Figs. 1 and 2. In the antiadiabatic limit the effective interaction as function of g is monotonically decreasing with g if the condition for pairing, Eq. (31) or (32), is not satisfied, while if it is satisfied it has a (negative) minimum for a finite g that decreases as U decreases below the limits given by Eqs. (31) and (32).

For an infinite chain, the pair binding energy can be calculated exactly in the antiadiabatic limit.²⁷ The appendix of Ref. 27 gives an analytic expression for the pair binding energy ϵ_b in one dimension. The quantity U_{eff} defined by Eq. (29) calculated here should go to $-\epsilon_b$ as the cluster size increases. Figure 1 also shows results for $-\epsilon_b$ (dotted lines), which go to zero when the parameters satisfy the equality in condition, Eq. (32). The difference between the dotted and dashed lines gives the magnitude of finite size effects for the $N=4$ cluster. It can be seen that the qualitative behavior of $-\epsilon_b$ for the infinite chain and U_{eff} for the four-site chain is the same. The effect of finite size is to give a somewhat larger attraction; however, the condition for pair formation ($U_{eff} < 0$) is the same for the $N=4$ cluster and the infinite chain in the antiadiabatic limit (the dashed and dotted lines in Fig. 1 go to zero at the same value of g).

In Fig. 3 we show the phase diagrams for the $N=2$ and $N=4$ clusters indicating the region where pairing will occur for some finite frequency in this model. The solid lines show the results in the antiadiabatic limit, Eqs. (31) and (32). It can be seen that the region of parameter space where pairing occurs is substantially enlarged for finite frequency. Figure 4 shows the optimal frequency for pairing at the phase bound-

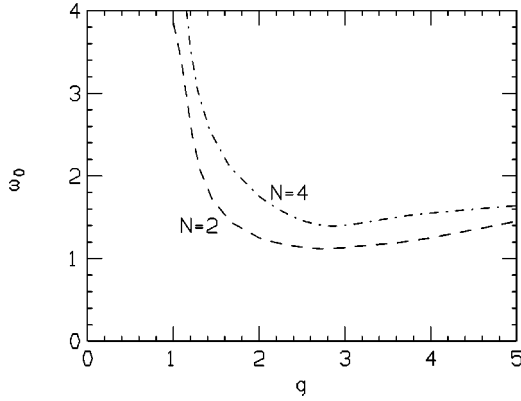


FIG. 4. Optimal frequency ω_0 that gives rise to pairing at the phase boundaries (dashed lines) of Fig. 3. As g decreases ω_0 increases and the phase boundary approaches the one in the antiadiabatic limit.

ary for pairing, for the $N=2$ and $N=4$ clusters. For large g , ω_0 increases slowly with g and is between 1 and 2 (in units of t). For decreasing g , ω_0 goes through a minimum and then diverges, in accordance with the fact that the phase boundary lines in Fig. 3 merge with the ones in the antiadiabatic limit as $g \rightarrow 0$. It should also be noted that for points away from the phase boundary the optimal frequency that gives maximum attraction can be considerably smaller than those shown in Fig. 4 [see, e.g., Fig. 2(a) for $U=4, g=4$ or Fig. 2(b) for $g=3, U=2$ where the optimal frequency is $\omega_0 \sim 0.5$].

B. Results for kinetic energy

The condensation energy in this model is known to be provided by lowering of kinetic energy in the antiadiabatic limit. Exact expressions for the pair kinetic energy for two bound holes in a one-dimensional chain are given in Ref. 27. Figure 5(a) shows exact results for the pair kinetic energy versus coupling constant g for the effective Hamiltonian, Eq. (12), for various values of U . Pairing occurs for couplings obeying the condition, Eq. (32), which for $U=0.8, 2$, and 3.2 corresponds to $g=0.5, 1$, and 2 , respectively. For g larger than those values the kinetic energy is given by the dashed line, lower than the solid line which would be the kinetic energy in the absence of pairing. Note that even though the kinetic energy of a pair is lower than that of the unbound holes, it still *decreases* in magnitude as the coupling g increases. Instead, the kinetic energy *lowering*, i.e., the difference between the kinetic energy of the pair and of the unbound holes, is nonmonotonic, peaking at an intermediate g , similarly to the pair binding energy given by $-U_{eff}$. Figure 5(b) shows the kinetic energy lowering per pair,

$$\Delta T = \langle T_p \rangle - \langle T_s \rangle, \quad (33)$$

and U_{eff} for the infinite chain, which is the negative of the pair binding energy ϵ_b calculated in Ref. 27. It can be seen that the two quantities follow similar behavior with coupling. In fact, their ratio is essentially constant as function of g for large g , as shown in Fig. 5(c). As the pair binding decreases,

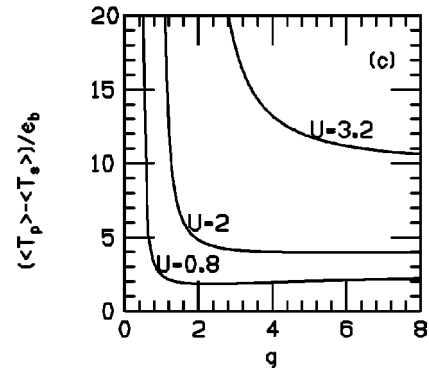
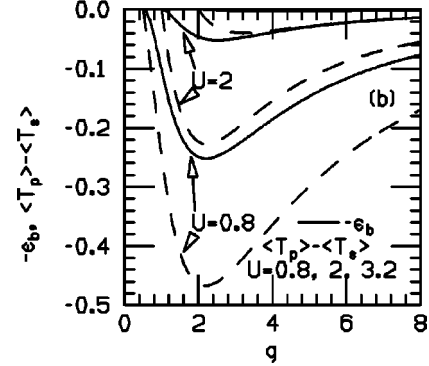
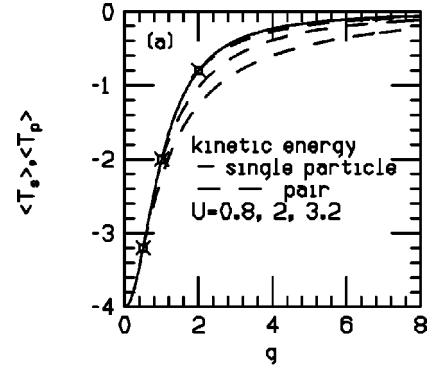


FIG. 5. Results for kinetic energy in the infinite chain in the antiadiabatic limit. (a) Kinetic energy of two unbound holes (solid line) and of a hole pair (dashed lines) vs g for various values of U . As g decreases, the dashed line joins the solid line (as indicated by the symbols) when pairs unbind, at $g = g_c$. Here g_c is 0.5, 1, and 2 for $U=0.8, 2$, and 3.2 , respectively. (b) Pair binding energy (solid lines) and kinetic energy lowering (dashed lines) for the infinite chain vs g for various U . At g_c , both quantities go to zero. (c) Ratio of kinetic energy lowering to pair binding energy vs g .

either because U increases or g decreases, both U_{eff} and the kinetic energy lowering go to zero. However, U_{eff} approaches zero quadratically²⁴ while the kinetic energy lowering approaches zero linearly, hence their ratio diverges as the pair binding energy goes to zero.

Note that the kinetic energy lowering upon pairing is always lower than $-\epsilon_b$. This indicates that the potential energy change is positive; that is, there is a potential energy cost upon pairing, given by

$$\Delta U_{pot} = (\langle T_s \rangle - \langle T_p \rangle) - \epsilon_b, \quad (34)$$

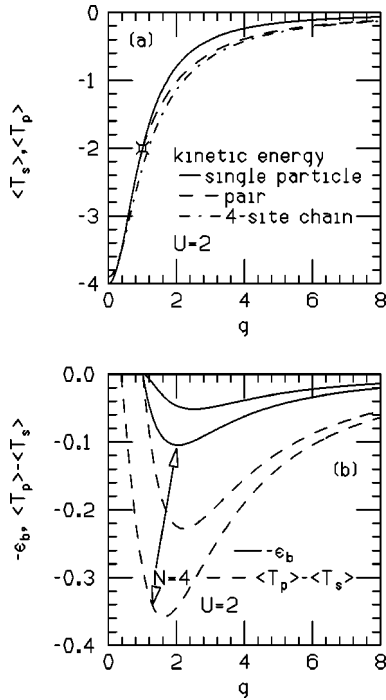


FIG. 6. Comparison of results for kinetic energy of $N=4$ chain and infinite chain in the antiadiabatic limit. In (a), the kinetic energy of two holes in the $N=4$ cluster (dash-dotted line) joins the infinite chain kinetic energy of the bound pair for large g (dashed line), and the kinetic energy of unbound holes for small g (solid line). (b) shows that finite-size effects similarly enhance the magnitude of pair binding energy and of kinetic energy lowering.

and the pair binding energy is smaller than would be expected from the magnitude of kinetic energy lowering. The potential energy cost arises from the increased effect of the on-site repulsion between members of a pair since the pair wave function has higher probability for site double occupancy.

In the infinite chain there is a sharp phase transition between the state where the pair is bound and where it is unbound, indicated by the points in Fig. 5(a) where the dashed lines join the solid line. In the finite chain of course there is no sharp transition but rather a smooth crossover. Figure 6(a) shows results for the kinetic energy for a pair of holes in the four-site chain in the antiadiabatic limit compared to the results for the infinite chain. As the coupling constant increases the four-site results cross over from the kinetic energy of unbound holes to the kinetic energy of the paired holes. When g goes to zero the kinetic energy of two holes in the four-site chain is slightly higher than the one for two unbound holes because of the effect of the on-site repulsion U ; this is of course a finite-size effect, and for larger clusters and a fixed number of holes it will become negligible in the regime where the holes are not bound. Figure 6(b) compares the kinetic energy lowering and the pair binding energy for the four-site chain in the antiadiabatic limit and the infinite chain for one case; it can be seen that both quantities follow similar behavior, and both are larger in magnitude than for the infinite chain. Note that in the finite chain kinetic energy lowering goes to zero for a smaller g than where U_{eff} goes to

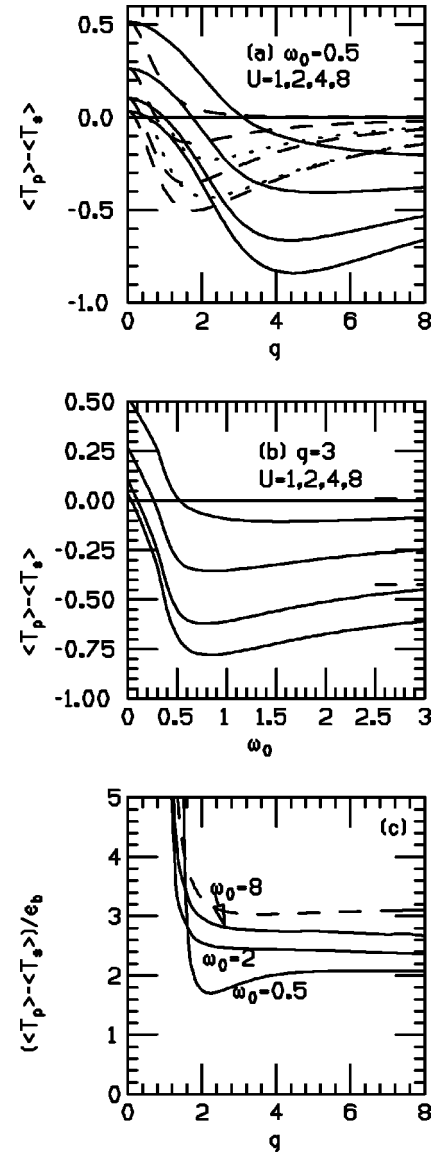


FIG. 7. Difference between kinetic energy of a pair and kinetic energy of two holes in the four-site chain (a) vs g for fixed ω_0 and (b) vs ω_0 for fixed g . The dashed and dotted lines in (a) give the results in the $\omega_0 \rightarrow \infty$ limit for the $N=4$ cluster and the infinite chain, respectively; the dashed lines in (b) give the results in the $\omega_0 \rightarrow \infty$ limit for the $N=4$ cluster. (c) Ratio of kinetic energy lowering to pair binding energy in four-site chain vs g for $U=2$ and various values of ω_0 . Note that the kinetic energy lowering upon pairing for small frequency is considerably larger for finite ω_0 than in the $\omega_0 = \infty$ limit.

zero; this would also occur in the infinite chain for finite hole density. We conclude from these results that the four-site cluster is appropriate to learn about the qualitative behavior of the kinetic energy for the infinite chain just as well as it is for the pair binding energy.

Hence we can now learn about the effect of finite frequency on kinetic energy lowering by studying the four-site chain. Figure 7(a) shows results for a finite small frequency, $\omega_0 = 0.5$, compared to the antiadiabatic limit $\omega_0 = \infty$. Just as for the effective interaction [Fig. 1(a)], the kinetic energy

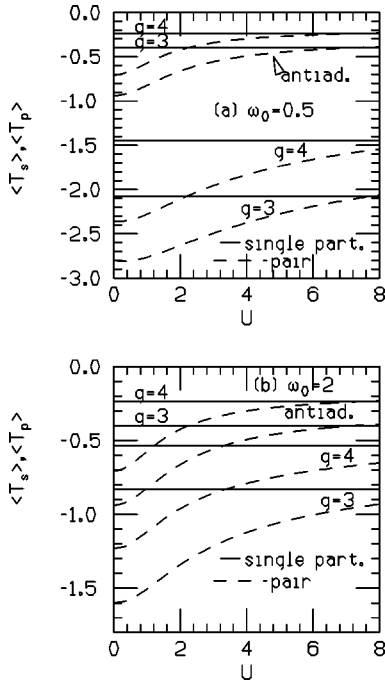


FIG. 8. Single particle (solid lines) and pair (dashed lines) kinetic energy vs U for $g=3$ and $g=4$ for (a) $\omega_0=0.5$ and (b) $\omega_0=2$. The results for $\omega_0 \rightarrow \infty$ are also shown. Both the single-particle and the pair kinetic energies are substantially lower for small ω_0 than for $\omega_0 = \infty$. The transition points where U_{eff} changes sign for $g=3$ and $g=4$ are, respectively, $U=3.6$ and $U=3.77$ for $\omega_0 = \infty$, $U=6.91$ and $U=10.1$ for $\omega_0=2$, and $U=5.57$ and $U=7.77$ for $\omega_0=0.5$.

lowering can be substantially larger for finite frequency than for infinite frequency, and the largest kinetic energy lowering occurs for larger g for small frequency. Similarly Fig. 7(b) shows kinetic energy lowering as function of frequency for fixed g . Similarly as the corresponding results for the effective interaction, Fig. 2(b), the kinetic energy lowering is largest in magnitude at a fairly low frequency and is considerably larger than in the antiadiabatic limit. The ratio of kinetic energy lowering to effective interaction for finite frequencies behaves similarly as in the antiadiabatic limit; this is shown for one case in Fig. 7(c).

In addition to kinetic energy lowering it is of interest to consider the effect of finite ω_0 on kinetic energy itself. Figure 8 shows results for single-hole and pair kinetic energy for finite ω_0 as function of the on-site repulsion U , compared with the limiting case $\omega_0 = \infty$. The difference between the dashed and solid lines is the kinetic energy lowering. It can be seen that relatively speaking the kinetic energy lowering is largest in the antiadiabatic limit, even though it is larger in magnitude for finite ω_0 .

In summary, we have seen that the effect of finite frequency is to enhance the pair binding energy and the kinetic energy lowering found in the antiadiabatic limit. From these results we conclude that the pair condensation energy in this dynamic Hubbard model also originates in kinetic energy lowering, i.e., “undressing.” As implied by the conductivity sum rule,^{29,30} lowering of kinetic energy should be accompanied by transfer of optical spectral weight from high to low

frequencies, as well as by transfer of spectral weight in the single-particle spectral function from high to low frequencies.³¹ The one and two-particle spectral functions for the model, Eq. (3), will be discussed in a separate paper.

IV. QUANTUM MONTE CARLO SIMULATIONS

With quantum Monte Carlo (QMC) methods one can study much larger systems than with exact diagonalization. We use the basis of σ_z eigenstates for the spin degrees of freedom, so that at every time slice i there are classical spins $\sigma_j(i)$ at every lattice site j . The partition function is

$$Z = \text{Tr} e^{-\beta H} = \text{Tr} \prod_{i=1}^L e^{-\Delta\tau H} = \text{Tr} \prod_{i=1}^L \sum_{\sigma_j(i)=\pm 1} e^{-\Delta\tau H(\sigma_j(i))}, \quad (35)$$

with $\Delta\tau = \beta/L$, L the number of time slices. There are two basic approaches to quantum Monte Carlo simulations, determinantal³² and world-line algorithms.³³

A. Determinantal Monte Carlo algorithm

For the determinantal algorithm one separates kinetic and potential energy terms in the Hamiltonian into the product of two exponentials and decouples the interaction term by a discrete Hubbard-Stratonovich transformation introducing auxiliary Ising variables which we call $\mu_j(i)$ here:³⁴

$$e^{-\Delta\tau U_j(i)n_{j\uparrow}n_{j\downarrow}} = \frac{1}{2} \sum_{\mu_j(i)=\pm 1} \exp\left(\lambda(\sigma_j(i))\mu_j(i)(n_{j\uparrow} - n_{j\downarrow}) - \frac{\Delta\tau U_j(i)}{2}(n_{j\uparrow} + n_{j\downarrow})\right), \quad (36a)$$

$$\cosh \lambda(\sigma_j(i)) = e^{\Delta\tau U_j(i)}, \quad (36b)$$

$$U_j(i) \equiv U(\sigma_j(i)) = U - 2g\omega_0\sigma_j(i). \quad (36c)$$

In contrast to the ordinary Hubbard model, the parameter λ here is not constant but depends on the local σ variable. For the transformation, Eq. (36), to be valid it is necessary that $U_j(i)$ be positive for all values of $\sigma_j(i)$, i.e., $U \geq 2g\omega_0$. Next one takes the trace over fermion degrees of freedom analytically to obtain the fermion determinant, and the Monte Carlo simulation proceeds by sampling the Ising spin degrees of freedom σ and μ at each space-time site. Even though negative weights may occur in this formulation, we do not expect that they will be very significant in the dilute regime of interest for this model.

The path integral formulation provided by Eqs. (35) and (36) makes the nature of this dynamic Hubbard model particularly apparent. The Hubbard U here has space-time fluctuations, with possible values $U_j(i) = U - 2g\omega_0$ and $U_j(i) = U + 2g\omega_0$. This fluctuating U corresponds to the different values that the on-site Coulomb repulsion between two electrons will take depending on the relative state of these electrons and embodies the physics of intra-atomic electronic correlation (at least for nondegenerate atomic orbitals). In a more realistic dynamic Hubbard model the Hubbard U will

take a continuum of different values. The energy scale that determines the fluctuations in U , ω_0 in this case, is a one-electron energy scale that reflects the cost in one-electron energy as the electrons sample the various atomic states to reduce the magnitude of their intra-atomic Coulomb repulsion.

The determinantal algorithm can be used for the lattice problem as well as for impurity problems and as part of the dynamical mean-field theory solution of the model. This will be deferred to future work. Here we will instead use the world-line QMC algorithm.

B. World-line Monte Carlo algorithm

The world-line Monte Carlo algorithm can be used if the system is one dimensional so that no negative-weight problems arise. The partition function is written as

$$Z = \text{Tr} \prod_{i=1}^L e^{-\Delta\tau \sum_j H_j} e^{-\Delta\tau H_{kin}^e} e^{-\Delta\tau H_{kin}^o}, \quad (37)$$

where the kinetic energy part of the Hamiltonian was decoupled in terms involving even and odd sublattices. The trace in Eq. (37) is performed by introducing intermediate states in the spin σ_z representation and the fermion occupation number representation in the usual way. In addition to moving fermion world lines and flipping individual σ spins we also use composite moves consisting in moving a fermion world line and flipping the spins at the sites where the fermion occupation is changing. These moves are necessary to achieve equilibration in the strong-coupling regime.

Figure 9 shows typical world-line configurations for two holes and the associated boson field in a strong-coupling regime, with $g=3$ and $\omega_0=2$. We start the holes far from each other, in the first snapshot shown (a) after several hundred sweeps they are still far apart and the world lines are rather straight, corresponding to large hole effective mass. After several more hundred sweeps the holes bind in a bipolaron, as seen in Fig. 9(b). The bipolaron has a smaller effective mass, as indicated by the larger transverse motion of the world lines in the timelike direction. These pictures clearly show that upon pairing the carriers become more mobile in this model.

The relation between pair formation and increase in pair mobility is shown even more clearly in Fig. 10. Figure 10(a) shows the kinetic energy of a pair as a function of Monte Carlo sweeps. Each Monte Carlo ‘‘step’’ in this figure gives an average over 30 consecutive sweeps. It can be seen that after approximately 100 steps the kinetic energy becomes lower. At the same time, as Fig. 10(b) shows, the average distance between the holes decreases dramatically as the pair is formed.

When the number of holes is increased in the system it is found in the BCS solution in the antiadiabatic limit that the tendency to pairing decreases and the coherence length of the pairs increases until they eventually dissociate at a critical hole concentration. Similar behavior is found in exact diagonalization of finite systems in the antiadiabatic limit. We find here that similar behavior is seen qualitatively in Monte

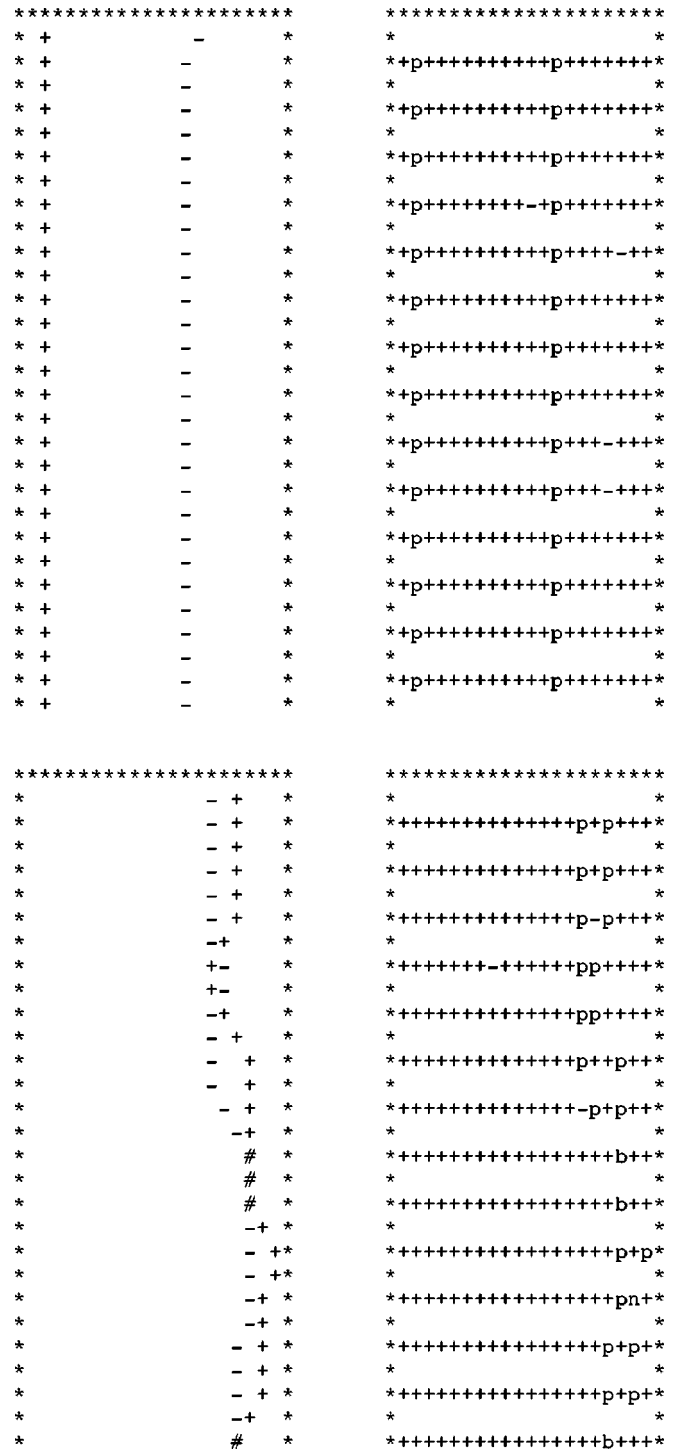


FIG. 9. Snapshots of Monte Carlo configurations for an $N=20$ site lattice with $L=40$ time slices. $\Delta\tau=0.25$, $g=3$, and $\omega_0=2$. The left-side panel show the hole world lines; the right-hand panel indicates the boson (spin) configuration. At the sites where the hole occupation is 1 (2), the boson configuration is denoted by p (b) if the boson state is $|-\rangle$, which is the low-energy configuration, and by n if it is $|+\rangle$. In (a), after a few hundred sweeps, the holes are separate and heavy; in (b), after several more hundred sweeps, the holes are bound and lighter (world lines fluctuate more in time direction).

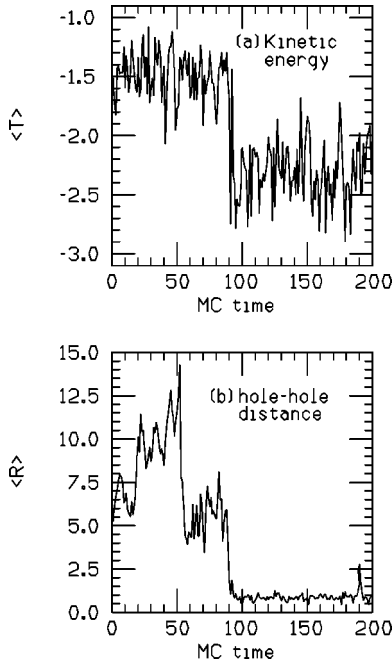


FIG. 10. Kinetic energy of two holes (a) and hole-hole distance (b) as function of “Monte Carlo time.” The unit of time is 30 Monte Carlo sweeps. $N=20$, $L=40$, $\Delta\tau=0.25$, $g=3$, and $\omega_0=1$. After about 100 steps the hole-hole distance decreases drastically as the holes become bound (b), and at the same time the kinetic energy becomes lower (a).

Carlo simulations for finite frequency. As an example, Fig. 11 shows snapshots of configurations for 6 holes in a 20-site system, i.e., hole concentration $n_h=0.15$. The system is started in a disordered configuration, after several thousand sweeps it could be seen in snapshots such as Fig. 11(a) that three well-defined pairs are formed; however, continuing the run, configurations like Fig. 11(b) appear, where pairs overlap and the distance between members of a pair (i.e., the coherence length) increases. Continuing this run the pairs dissociate completely, later they form again. These snapshots suggest that for these parameters the system is close to the pair unbinding transition (it is not clear on which side). The dependence of critical hole concentration on frequency ω_0 is unknown and an interesting subject for further study. The fact that the effective attraction increases for finite frequency in the exact diagonalization study suggests that the critical hole concentration may be larger for finite frequency than in the $\omega_0 \rightarrow \infty$ limit.

To detect a superconducting transition in Monte Carlo simulations it is considerably simpler to use a grand canonical ensemble formulation as in the determinantal Monte Carlo methods; in world-line Monte Carlo simulations, measurement of pairing correlation functions would involve breaking world lines which leads to large fluctuations.³³ We can, however, get some information on pair binding with the world-line method by consideration of the kinetic energy. As seen in Fig. 8, the kinetic energy increases gradually in the four-site system as the on-site repulsion increases. Figure 12 shows the behavior of kinetic energy from Monte Carlo simulations on lattices of size $N=8$ and $N=12$, as well as

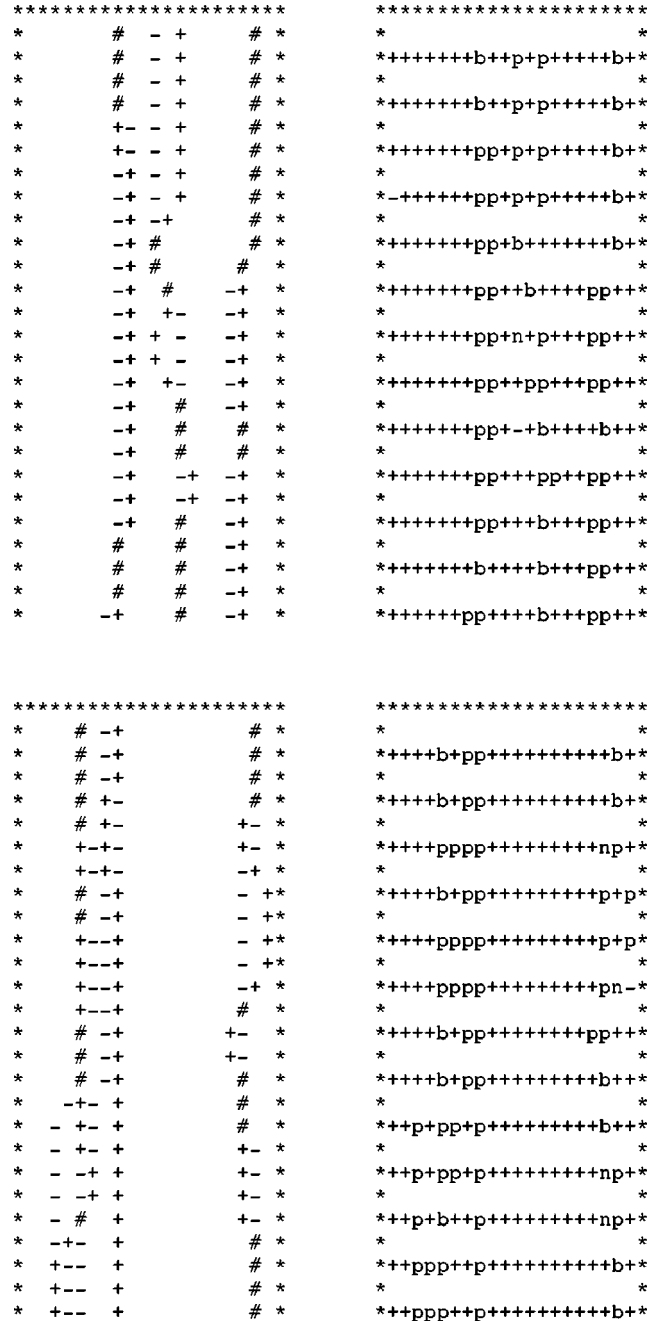


FIG. 11. Snapshots for 6 holes in a 20-site chain. $L=40$, $\Delta\tau=0.25$, $g=3$, and $\omega_0=2$. In the first picture (a) three well-defined pairs are seen; in (b) the pairs overlap and the distance between members of a pair (“coherence length”) increases.

for the static (conventional) Hubbard model ($g=0$). For the static Hubbard model there is a small dependence of kinetic energy on U , which is due to finite-size effects. Instead, for the dynamic Hubbard model there is a large increase in kinetic energy as U increases from small values, due to the progressive unbinding of the pair. For sufficiently large U the pair unbinds and the dependence of kinetic energy on U is weak as in the static Hubbard model. For the $N=12$ cases a fairly sharp kink in the kinetic energy indicates the transition point.

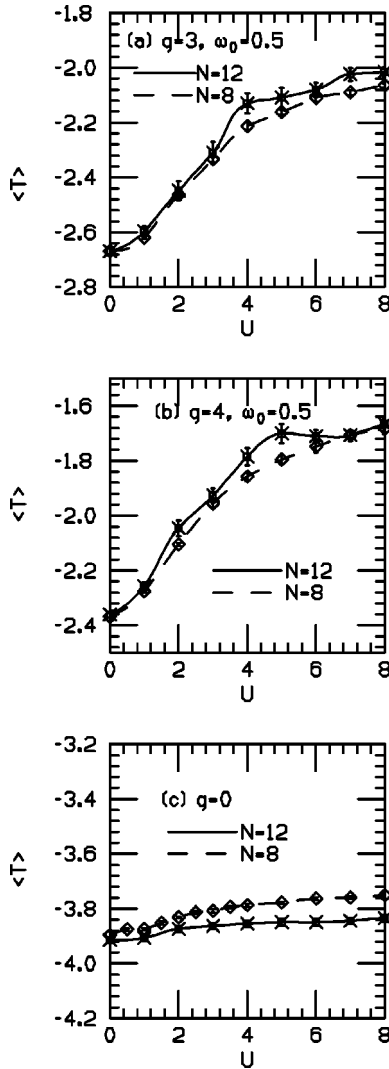


FIG. 12. Kinetic energy vs on-site repulsion U from Monte Carlo simulations of dynamic Hubbard model (a), (b), and of static (conventional) Hubbard model ($g=0$) (c).

Similarly the existence of pairing can be seen in density-density correlation functions. Figures 13(a) and 13(b) show on-site and nearest-neighbor hole-hole density correlations for the static Hubbard model and the dynamic cases of Fig. 12. The on-site correlation is much larger in the dynamic case, and approaches the static case values only for large U . The nearest-neighbor correlation in the dynamic case is much larger than in the static case and first increases as U increases, due to the rapid decrease of the on-site correlation. Note also that for large U the nearest-neighbor correlation is still considerably larger than in the static model, indicating that when the on-site double occupation is essentially suppressed, retardation gives rise to an effective nearest-neighbor attraction. This can be easily understood from second-order strong-coupling perturbation theory.

Electrons behave very different from holes in this model. In Fig. 14 we show snapshots of hole world-line configurations when the band is almost full with holes, i.e., almost empty with electrons. This is the mirror image of the case shown in Fig. 9. Here we start the simulation with two elec-

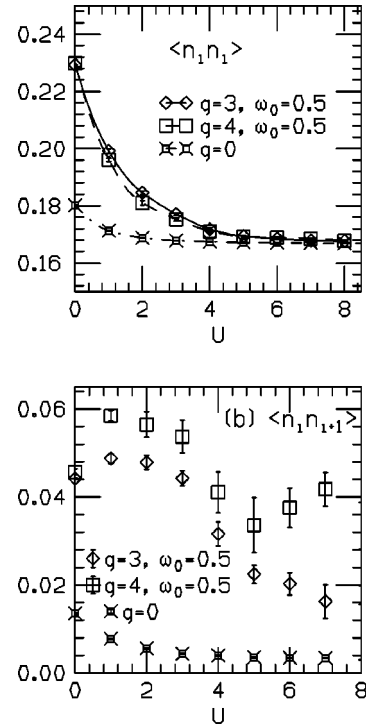


FIG. 13. (a) On-site and (b) nearest-neighbor density-density correlations for dynamic and static Hubbard model, $N=12$ sites.

trons on the same site, and after some sweeps the electrons separate. Furthermore, in contrast to Fig. 9, the quasiparticle world lines show much larger fluctuations in the time direction, indicating a smaller electron effective mass. The contrast between Figs. 14 and 9 clearly displays the intrinsic electron-hole asymmetry of this dynamic Hubbard model. The kinetic energy in this case shows almost no dependence on U , as expected, in contrast to the case shown in Fig. 12.

In summary, the results of these Monte Carlo simulations support the picture obtained from exact diagonalization of small systems: the dynamic Hubbard model is an effective way to obtain hole pairing driven by kinetic energy lowering in repulsive fermion systems.

V. COMPARISON WITH RESULTS FOR A HOLSTEIN-LIKE MODEL

The conventional electron-boson models studied in the past involve coupling of a boson degree of freedom to the electronic charge density rather than to the double occupancy. Even though it does not necessarily follow, in their simplest form these models are electron-hole symmetric. We consider here one such model with site Hamiltonian

$$H_i = \omega_0 \sigma_x^i + g \omega_0 \sigma_z^i [n_{i\uparrow} + n_{i\downarrow} - 1] + U n_{i\uparrow} n_{i\downarrow} \quad (38)$$

as a generic model in that class. This model should be similar to the Holstein model,²⁵ where the spin-1/2 degree of freedom is replaced by a harmonic oscillator. Diagonalization of the site Hamiltonian yields eigenvalues

$$\epsilon(0) = \epsilon(2) = -\epsilon(\bar{0}) = -\epsilon(\bar{2}) = -\omega_0 \sqrt{1+g^2}, \quad (39a)$$

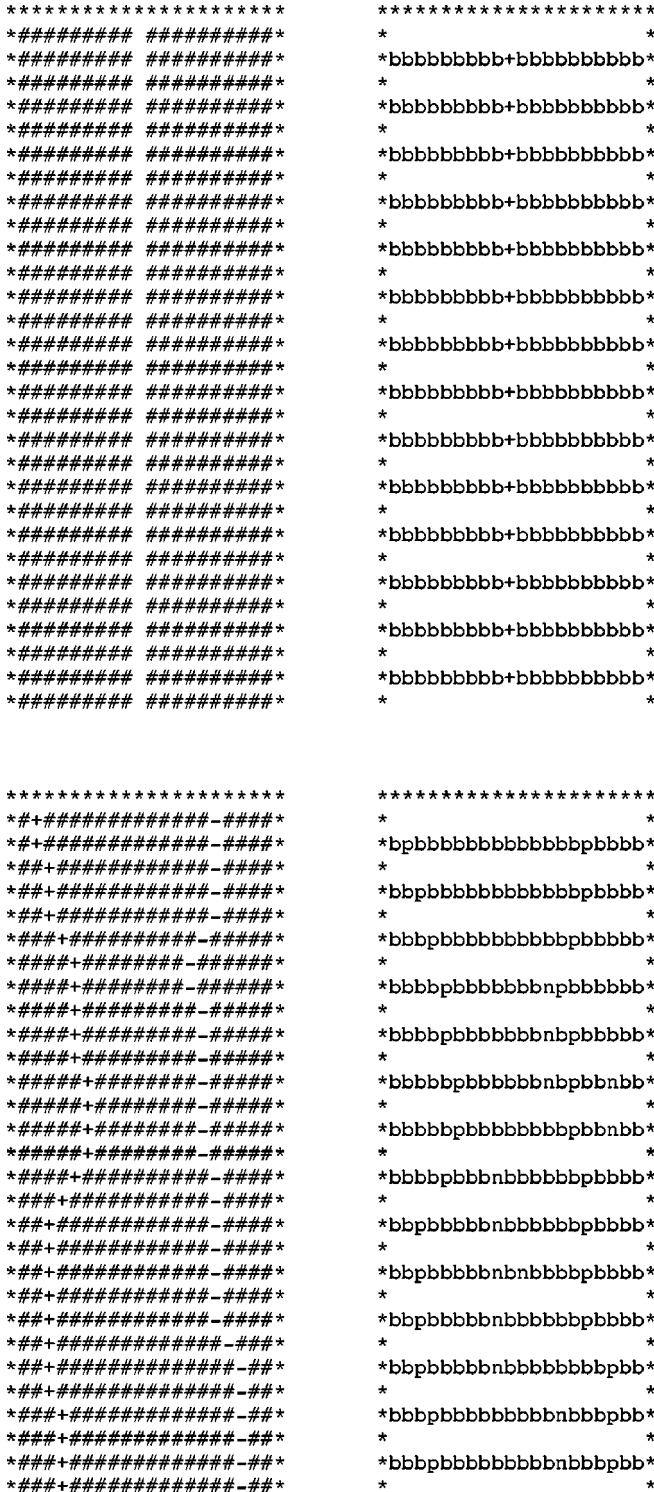


FIG. 14. Snapshots of Monte Carlo configurations when the band is almost full with holes, with only two electrons. The convention and parameters are the same as in Fig. 9. The simulation is started with the two electrons on the same site (top panel); after a few sweeps (bottom panel) the electrons separate and are light, as illustrated by the large fluctuations of the world lines in the time direction.

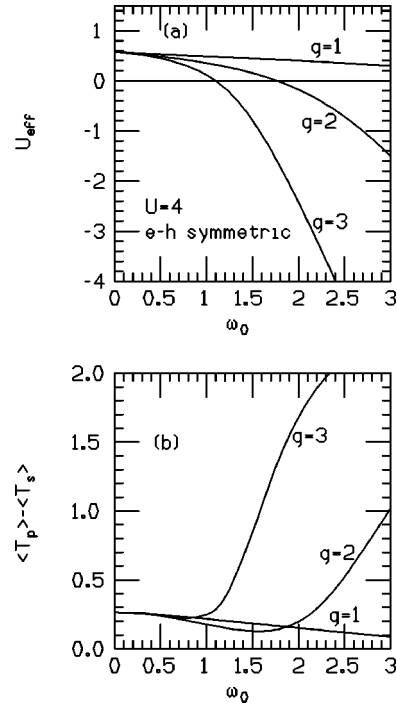


FIG. 15. Exact diagonalization results for Holstein-like model, Eq. (39). (a) Effective interaction and (b) difference between kinetic energy of a pair and kinetic energy of two holes in the four-site chain vs frequency ω_0 for $U=4$ and various values of g . The kinetic energy increases rapidly as the effective interaction becomes more attractive, in contrast to the behavior found in the dynamic Hubbard model.

$$\epsilon(1) = -\epsilon(\bar{1}) = -\omega_0 \quad (39b)$$

and eigenvectors of the form Eq. (4), with

$$u(0) = v(2) = \frac{1}{\sqrt{2}} \sqrt{1 + \frac{g}{\sqrt{1+g^2}}}, \quad (40a)$$

$$v(0) = u(2) = -\frac{1}{\sqrt{2}} \sqrt{1 - \frac{g}{\sqrt{1+g^2}}}, \quad (40b)$$

$$u(1) = -v(1) = \frac{1}{\sqrt{2}} \quad (40c)$$

and effective on-site interaction

$$U_{eff} = U - 2\omega_0(\sqrt{1+g^2} - 1). \quad (41)$$

The overlap matrix element between ground-state wave functions is

$$S = \langle 0|1 \rangle = \langle 1|2 \rangle = \sqrt{\frac{1}{2} \left(1 + \frac{1}{\sqrt{1+g^2}} \right)} \quad (42)$$

and ranges between 1 for $g=0$ to $1/\sqrt{2}$ for $g \rightarrow \infty$, so that it never becomes small as in the previous case.

Figure 15 shows results of exact diagonalization for an $N=4$ cluster. As a function of frequency, the effective interaction becomes less attractive as ω_0 decreases, in contrast to the behavior found for the dynamic Hubbard model. Further-

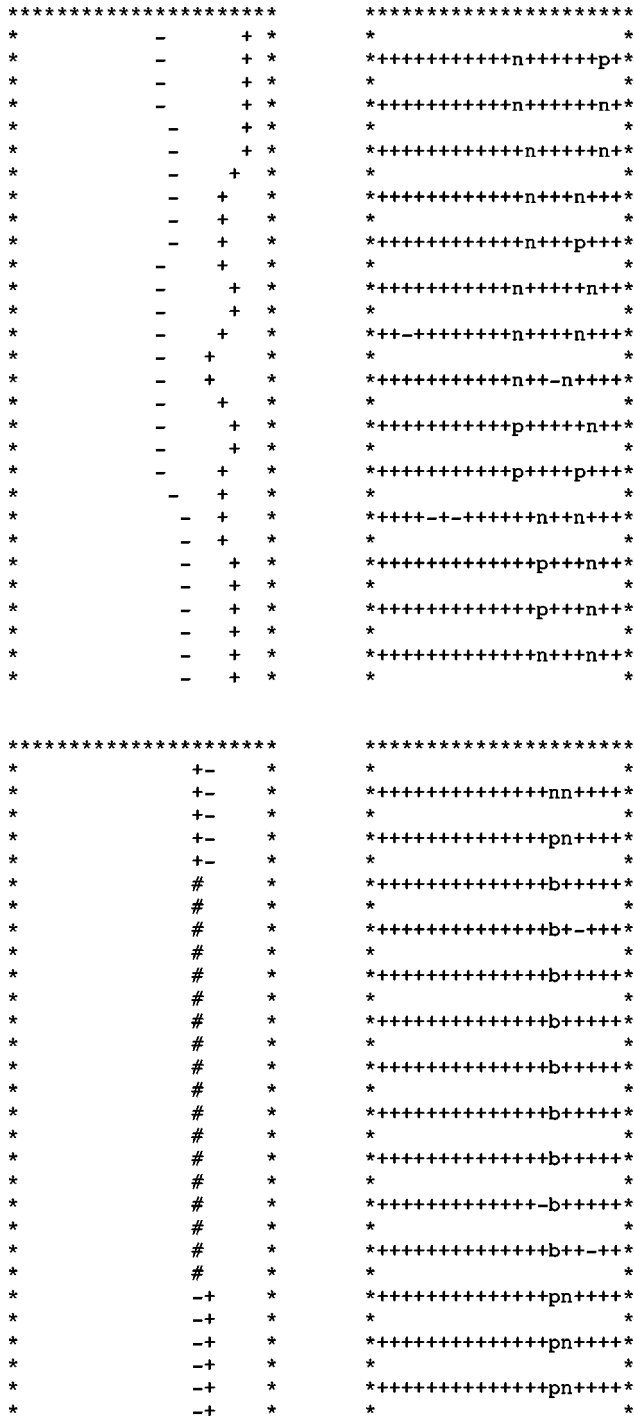


FIG. 16. Snapshots of Monte Carlo configurations for the Holstein-like model for an $N=20$ site lattice with $L=40$ time slices. $\Delta\tau=0.25$, $g=3$, $\omega_0=2$, and $U=4$. Same conventions as in Fig. 9. After a few initial sweeps the holes are still separate and light (upper panels); after several more sweeps (lower panels) the holes are bound and heavier (world lines fluctuate less in the time direction), in contrast to the behavior seen in Fig. 9.

more, the kinetic energy increases as ω_0 increases and the effective attraction increases, as shown in Fig. 15(b). Hence in this model pairing gives rise to kinetic energy *increase* and the pair condensation energy originates in the larger po-

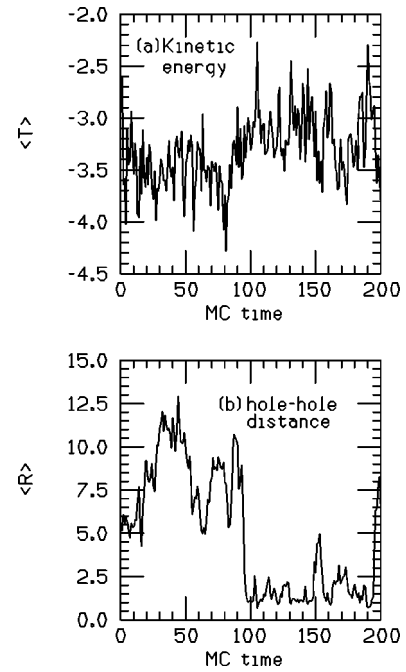


FIG. 17. Kinetic energy of two holes (a) and hole-hole distance (b) as function of “Monte Carlo time” for the Holstein-like model. The unit of time is 15 Monte Carlo sweeps. $N=20$, $L=40$, $\Delta\tau=0.25$, $g=3$, $\omega_0=1$, and $U=3$. After about 100 steps the hole-hole distance decreases drastically as the holes become bound (b), and at the same time the kinetic energy increases (a), in contrast to the behavior seen in Fig. 10.

tential energy decrease, which is precisely opposite to the behavior in the dynamic Hubbard model.

Figure 16 shows typical world-line configurations for two holes in this model. Similarly to Fig. 9, we start the holes far from each other; in the first snapshot they are still separate and after several sweeps a pair is formed. Here the world lines for the pair are rather straight, corresponding to large effective mass, while the single holes exhibit larger transverse motion of the world lines, indicating lighter quasiparticles. This is qualitatively different to the behavior in the dynamic Hubbard model (Fig. 9), where the carriers became lighter when they paired.

The relation between pair formation and pair mobility is also shown in Fig. 17, to be compared with Fig. 10 for the dynamic Hubbard model. Initially the hole-hole distance is large and the kinetic energy is low. When the pairs form after approximately 100 Monte Carlo “steps” the hole-hole distance decreases drastically and the kinetic energy increases, again in qualitative contrast with the behavior found in the dynamic Hubbard model.

Finally, Fig. 18 shows the behavior of the average kinetic energy and of density-density correlations versus on-site repulsion U for the Holstein-like model. As indicated by Fig. 15, the effective interaction becomes attractive for $g=3$ and $\omega_0=1$ when $U\sim 4$. This is confirmed by the results of Fig. 18. The on-site density-density correlation increases sharply as U is decreased below 4, indicating pair formation. At the same time, the kinetic energy increases sharply when the pair

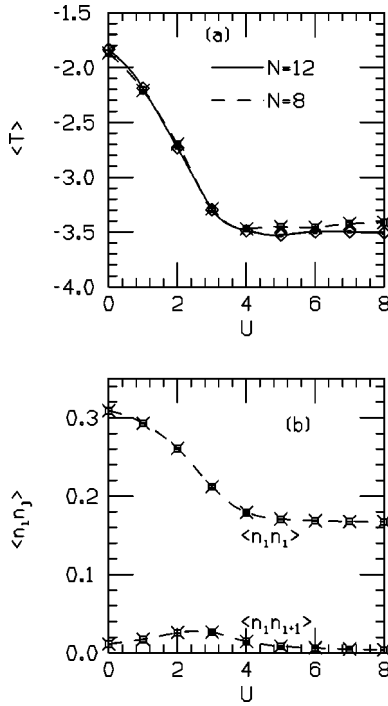


FIG. 18. (a) Kinetic energy and (b) on-site and nearest-neighbor density-density correlation vs on-site repulsion U from Monte Carlo simulations of the Holstein-like model with $N=12$. In (a) results for $N=8$ are also shown; for (b) the size dependence is negligible. As U decreases and pairs form, the on-site correlations increase and the kinetic energy increases, in contrast to the behavior seen in Figs. 12 and 13 for the dynamic Hubbard model.

forms, again in stark contrast to the behavior of the dynamic Hubbard model seen in Figs. 12 and 13. The nearest-neighbor density-density correlation first increases as U increases from 0, indicating that the pair wave function evolves from describing on-site pairing to more extended pairing and then decreases for larger U as the pair dissociates.

In summary, these results suggest that the conventional electron-hole symmetric models and dynamic Hubbard models define two rather different “universality classes.” Both types of models can describe pairing, with qualitatively different features.

VI. RELATION TO REAL ATOMS

In the dynamic Hubbard model considered in this paper, the on-site repulsion takes the values $U-2g\omega_0$ and $U+2g\omega_0$ when the auxiliary spin at the site points up and down, respectively, in a σ_z representation. More generally, for the spin in a superposition of these states the on-site repulsion will take values intermediate between these extremes. The “effective” on-site repulsion defined by

$$U_{eff}(\text{site}) = E(2) + E(0) - 2E(1), \quad (43)$$

with $E(n)$ the site energy with n electrons (or holes), is simply U . The reason a fluctuating U is needed to represent a real atom is that the wave function of two electrons in an

orbital is not simply the product of the single-electron wave functions in the singly occupied atom,³ but rather a superposition

$$\Psi(r_1, r_2) = \sum_{n,m} C_{nm} \varphi_n(r_1) \varphi_m(r_2), \quad (44)$$

where $\{\varphi_n(r)\}$ is a complete set of single-electron wave functions. The fluctuating values of U can be thought of as the different values that the electron-electron repulsion will take for one electron in $\varphi_n(r)$ and the other electron in $\varphi_m(r)$, for all n, m for which C_{nm} is not zero. The frequency ω_0 represents the energy scale of electronic excitations in the atom, i.e., the eigenenergies of the wave functions $\{\varphi_n(r)\}$.

More specifically, for the particular case of $1s$ orbitals in a hydrogenic atom of ionic charge Z , the “bare” on-site repulsion for two electrons in the $1s$ orbital is

$$U_1 = 17Z \text{ eV}. \quad (45)$$

This corresponds in our model to the on-site repulsion when the boson is not allowed to relax, Eq. (8), or approximately $U+2g\omega_0$. In the Hartree approximation, the orbital expands to $\bar{Z} = Z - 5/16$ upon double occupation, and the repulsion between two electrons in these expanded orbitals is Eq. (45) with Z replaced by \bar{Z} , i.e.,

$$U_2 = 17 \left(Z - \frac{5}{16} \right) \text{ eV} = U_1 - 5.31 \text{ eV}. \quad (46)$$

This would roughly correspond to the “minimum” on-site repulsion in our model, $U-2g\omega_0$. Finally, the effective on-site repulsion in the Hartree approximation, taking into account the cost in single-particle energy upon orbital expansion, is

$$U_3 = 17 \left(Z - \frac{5}{32} \right) \text{ eV} = U_1 - 2.66 \text{ eV} \quad (47)$$

precisely halfway between the values, Eqs. (45) and (46), and this would correspond to the effective site U in our model, which is just U , also precisely halfway between the minimum and maximum values. Summarizing,

$$U_1 = 17Z \text{ eV} = U + 2g\omega_0, \quad (48a)$$

$$U_2 = U_1 - 5.31 \text{ eV} = U - 2g\omega_0, \quad (48b)$$

$$U_3 = U_1 - 2.66 \text{ eV} = U, \quad (48c)$$

so that for this case we have simply

$$g\omega_0 = 1.33 \text{ eV} \quad (49)$$

independent of Z .

The frequency ω_0 is related to excitation energies of the atom; hence, we expect the dependence on ionic charge

$$\omega_0 = cZ^2, \quad (50)$$

which implies from Eq. (49) that g increases as the ionic charge Z decreases. This is in accordance with the fact that the overlap

$$S = \langle 0|1 \rangle = \frac{1}{\sqrt{1+g^2}} \quad (51)$$

decreases as g increases; in the Hartree approximation, this overlap corresponds to the overlap of the expanded single-electron orbital with the nonexpanded one and is given by

$$S = \frac{\left(1 - \frac{5}{16Z}\right)^{3/2}}{\left(1 - \frac{5}{32Z}\right)^3}, \quad (52)$$

which decreases to zero as $Z \rightarrow 0.3125$.

Strictly speaking our dynamic Hubbard model will be a valid representation of the real atom only in the parameter regime where

$$U - 2g\omega_0 > 0, \quad (53)$$

because the atomic Coulomb integral for any two orbitals φ_n, φ_m has to be positive. Even with the constraint, Eq. (53), a wide range of parameters in the model exists where pairing will occur, as can be inferred from the numerical results in the previous sections. For example, from Fig. 1(a) we see that for $\omega_0=0.5, U=8$, pairing occurs for $g > 4$; the condition, Eq. (53), is satisfied in this case up to $g=8$, and for $g \sim 4$ the fluctuations in the on-site U are about 50%. As the frequency gets smaller, the relative fluctuations in U needed to obtain pairing decrease. For example, from Fig. 2(a) we find that for $U=4, g=4$, pairing occurs for $\omega_0 > 0.12$, which corresponds to fluctuations in U of only 25% (between $U=3$ and $U=5$). If the U was not fluctuating but fixed, no pairing occurs in the model unless $U < 0$. In other words, the “equivalent U ” in a model with fixed U is not only smaller than the average U in the fluctuating case but it is smaller than the smallest value that the fluctuating U attains in these cases.

Note that as Z in the atom decreases, the on-site bare U decreases [Eq. (45)]; the parameter ω_0 should decrease according to Eq. (50), and correspondingly g should increase [Eq. (49)]. As seen in Fig. 2(b), as U decreases a smaller ω_0 is required to give pairing, and as seen in Fig. 2(a) as g increases also a smaller ω_0 is needed for pairing. We conclude from our results for the model system and the relationship with the real atom that smaller values of Z yield the most favorable conditions for pairing in this dynamic Hubbard model.

VII. DISCUSSION

We have studied numerically some properties of a dynamic Hubbard model, where the value of the on-site repulsion U depends on the state of an auxiliary boson degree of freedom. In the model studied in this paper the boson is a spin-1/2 degree of freedom, with excitation energy ω_0 . It will be of interest to study other similar models with other boson degrees of freedom such as other versions of the spin-1/2 model,¹ higher spin variables or harmonic oscillators, or purely electronic models with more than one orbital per site;³

we believe the qualitative physics will be similar. Furthermore, “extended” dynamic Hubbard models, with more than on-site interactions, should be interesting to study.

These dynamic Hubbard models map onto the Hubbard model with correlated hopping in the antiadiabatic limit $\omega_0 \rightarrow \infty$, which is known to lead to pairing of holes and superconductivity for sufficiently large coupling constant g ; the purpose of this paper was to determine whether pairing still exists for finite ω_0 . Furthermore, in the antiadiabatic limit pairing is known to occur through kinetic energy lowering, and we examined whether the same physics occurs for finite ω_0 .

From both the exact diagonalization and the quantum Monte Carlo results we concluded that the same physics of the antiadiabatic limit persists for finite, and even small, ω_0 . Furthermore, the parameter regime where pairing occurs is larger for small ω_0 than for $\omega_0 \rightarrow \infty$. When ω_0 is small the kinetic energy is much lower than in the antiadiabatic limit, yet the magnitude of kinetic energy lowering upon pairing is similar to that in the antiadiabatic limit.

The $\omega_0 \rightarrow \infty$ limit of the model (Hubbard model with correlated hopping) is useful because its physics is rather transparent and because it allows for much simpler analytic and numerical treatments. However, strictly speaking the dynamic Hubbard model considered here is only a realistic representation of a real system for parameters where $U - 2g\omega_0 > 0$, which certainly does not hold in the antiadiabatic limit. Hence it is essential to establish that the properties of the model for small ω_0 and for $\omega_0 \rightarrow \infty$ are similar if one is to use the results obtained from the $\omega_0 \rightarrow \infty$ limit to understand the properties of a real system. We found that the model can give rise to pairing even in parameter ranges where the fluctuating U attains only positive values, which implies that an “equivalent” fixed U in those cases would be smaller than the lower bound of the range within which U fluctuates.

We contrasted the behavior found in the dynamic Hubbard model with that of an electron-hole symmetric Holstein-like model. In the latter model, which we suggest is representative of a wide range of model Hamiltonians that have been considered in the past to describe superconductivity, the physics found is qualitatively different: pairing is associated with lowering of potential energy and increase in kinetic energy, opposite to the behavior found in the dynamic Hubbard model. We suggest that these two models, each representative of an entire class of model Hamiltonians, are two different paradigms by which superconductivity can be achieved.³⁶ Whether either or both occur in nature is an unsettled question. The theory of hole superconductivity proposes that only the paradigm represented by the dynamic Hubbard model occurs in real materials.^{8,9}

We also discussed briefly the relation between the dynamic Hubbard model considered here and a real hydrogen-like atom for $1s$ electrons in the Hartree approximation. Clearly such relation should be qualitatively similar for more accurate representations of the two-electron wave function such as the Hylleraas wave function,³ as well as for electrons in other atomic orbitals. We found that a smaller value of the ionic charge Z yields more favorable conditions for pairing

for several different reasons: (1) it leads to smaller on-site repulsion U , (2) it leads to larger coupling g , which leads to larger “dressing” of quasiparticles in the normal state and to larger “undressing,” hence larger energy lowering, as quasiparticles pair, and (3) it leads to smaller frequency scale ω_0 , which according to the results of this paper is favorable to pairing as U becomes smaller and g becomes larger. In addition, smaller Z is also favorable because it leads to larger orbital overlap between atoms, hence larger bare hopping t , which increases the overall scale of the pairing interaction calculated in this paper.²¹ It will be interesting to perform detailed analysis of the connection between this and other dynamic Hubbard models and electrons in various orbitals in real atoms.

The results presented here are only a first step in the understanding of this and other dynamic Hubbard models. Analytically, both strong- and weak-coupling expansions should

be feasible and of interest. Powerful numerical techniques that have been extensively used for the static Hubbard model and other related models such as the Holstein model can and should be brought to bear on this class of models. In particular, density matrix renormalization group³⁵ and determinantal Monte Carlo methods should allow for the study of larger systems as a function of model parameters and hole concentration to determine the range of parameters where hole pairing occurs. The dynamical mean-field method combined with a Monte Carlo “impurity” method should be a very fruitful approach to deal with this class of models.³⁷ In particular, it will be of great interest to understand quantitatively the processes of spectral weight transfer in one- and two-particle Green’s functions that are expected to occur in this class of models upon transition to the superconducting state,^{30,31} which are of interest in connection with photoemission³⁸ and optical experiments³⁹ in superconducting materials.

-
- ¹J.E. Hirsch, Phys. Lett. A **134**, 451 (1989); Physica B **199&200**, 366 (1994).
- ²J.E. Hirsch, Phys. Rev. Lett. **87**, 206402 (2001).
- ³J.E. Hirsch, Phys. Rev. B **65**, 184502 (2002)
- ⁴J. Hubbard, Proc. R. Soc. London, Ser. A **276**, 238 (1963).
- ⁵J.E. Hirsch and S. Tang, Phys. Rev. B **40**, 2179 (1989).
- ⁶J.E. Hirsch, Phys. Rev. B **47**, 5351 (1993).
- ⁷J.E. Hirsch, Phys. Rev. B **43**, 11 400 (1991).
- ⁸J.E. Hirsch, Phys. Rev. B **48**, 3327 (1993); **48**, 3340 (1993); **48**, 9815 (1993).
- ⁹J.E. Hirsch, Physica C **158**, 326 (1989); Phys. Lett. A **138**, 83 (1989); in *High Temperature Superconductors: Relationship Between Properties, Structure, and Solid-State Chemistry*, edited by J. R. Jorgensen, K. Kitazawa, J. M. Tarascon, M. S. Thompson, and J. B. Torrance, Mater. Res. Soc. Symp. Proc. No. 156 (Materials Research Society, Pittsburgh, 1989), p. 349; Physica C **341-348**, 213 (2000).
- ¹⁰*The Hubbard Model: A Reprint Volume*, edited by A. Montorsi (World Scientific, Singapore, 1992), and references therein.
- ¹¹*The Hubbard Model: Its Physics and Mathematical Physics*, edited by Dionys Baeriswyl *et al.* (Plenum, New York, 1995) and references therein.
- ¹²J.E. Hirsch and F. Marsiglio, Phys. Rev. B **41**, 2049 (1990).
- ¹³J.E. Hirsch and F. Marsiglio, Phys. Rev. B **39**, 11 515 (1989); Physica C **162-164**, 591 (1989).
- ¹⁴R. Micnas, J. Ranninger, and S. Robaszkiewicz, Phys. Rev. B **39**, 11 653 (1989).
- ¹⁵J. Appel, M. Grodzicki, and F. Paulsen, Phys. Rev. B **47**, 2812 (1993).
- ¹⁶L. Arrachea, A.A. Aligia, E. Gagliano, K. Hallberg, and C. Balseiro, Phys. Rev. B **50**, 16 044 (1994).
- ¹⁷M. Airolidi and A. Parola, Phys. Rev. B **51**, 16 327 (1995).
- ¹⁸H.Q. Lin and J.E. Hirsch, Phys. Rev. B **52**, 16 155 (1995).
- ¹⁹M. Quaiser, A. Schadschneider, and J. Zittartz, Europhys. Lett. **32**, 179 (1995); F.C. Alcaraz and R.Z. Bariev, Phys. Lett. A **240**, 247 (1998).
- ²⁰G.I. Japaridze and E. Muller-Hartmann, Ann. Phys. (Leipzig) **3**, 163 (1994).
- ²¹F. Marsiglio and J.E. Hirsch, Phys. Rev. B **41**, 6435 (1990).
- ²²F. Marsiglio and J.E. Hirsch, Physica C **159**, 157 (1989); J.E. Hirsch, Phys. Rev. B **59**, 11 962 (1999).
- ²³J.E. Hirsch and F. Marsiglio, Phys. Rev. B **62**, 15 131 (2000) and references therein.
- ²⁴F. Marsiglio and J.E. Hirsch, Physica C **171**, 554 (1990).
- ²⁵T. Holstein, Ann. Phys. (N.Y.) **8**, 325 (1959).
- ²⁶J.E. Hirsch, Physica C **179**, 317 (1991).
- ²⁷J.E. Hirsch and F. Marsiglio, Phys. Rev. B **45**, 4807 (1992).
- ²⁸J.E. Hirsch and F. Marsiglio, Physica C **331**, 150 (2000).
- ²⁹J.E. Hirsch, Physica C **199**, 305 (1992).
- ³⁰J.E. Hirsch, Physica C **201**, 347 (1992).
- ³¹J.E. Hirsch, Phys. Rev. B **62**, 14 487 (2000); **62**, 14 498 (2000).
- ³²R. Blankenbecler, D.J. Scalapino, and R.L. Sugar, Phys. Rev. D **24**, 2278 (1981).
- ³³J.E. Hirsch, R.L. Sugar, D.J. Scalapino, and R. Blankenbecler, Phys. Rev. B **26**, 5033 (1982).
- ³⁴J.E. Hirsch, Phys. Rev. B **31**, 4403 (1985).
- ³⁵C. Zhang, E. Jeckelmann, and S.R. White, Phys. Rev. B **60**, 14 092 (1999).
- ³⁶J.E. Hirsch, Science **295**, 2226 (2002).
- ³⁷A. Georges, G. Kotliar, W. Krauth, and M.J. Rozenberg, Rev. Mod. Phys. **68**, 13 (1996).
- ³⁸H. Ding, J.R. Engelbrecht, Z. Wang, J.C. Campuzano, S.-C. Wang, H.-B. Yang, R. Rogan, T. Takahashi, K. Kadowaki, and D.G. Hinks, Phys. Rev. Lett. **87**, 227001 (2001).
- ³⁹H.J.A. Molegraaf, C. Presura, D. van der Marel, P.H. Kes, and M. Li, Science **295**, 2239 (2002); A.F. Santander-Syro, R.P.S.M. Lobo, N. Bontemps, Z. Konstantinovic, Z.Z. Li, and H. Raffy, cond-mat/0111539 (unpublished).